Dielectric and EPR investigations of stoichiometry and interface effects in silicon carbide nanoparticles

2006 J. Phys.: Condens. Matter 18 1143

(http://iopscience.iop.org/0953-8984/18/4/003)

INSTITUTE OF PHYSICS PUBLISHING JOURNAL OF PHYSICS: CONDENSED MATTER

J. Phys.: Condens. Matter **18** (2006) 1143–1155 doi:10.1088/0953-8984/18/4/003

Dielectric and EPR investigations of stoichiometry and interface effects in silicon carbide nanoparticles

M Tabellout[1], A Kassiba[1,3], S Tkaczyk[2], L Laskowski[2] and J Swiatek[2]

[1] Laboratoire de Physique de l'Etat Condensé, UMR CNRS 6087, Université du Maine, Avenue Olivier Messiaen, 72085 Le Mans cedex 9, France
[2] Institute of Physics, Akademia im. Jana DLugosza W Czestochowa Aleja Armii Krajowej 13/15-42201 Czestochowa, Poland

E-mail: kassiba@univ-lemans.fr

Received 24 July 2005
Published 9 January 2006
Online at stacks.iop.org/JPhysCM/18/1143

Abstract

The dielectric properties of non-stoichiometric silicon carbide nanoparticles (np-SiC), with a silicon-rich composition in the atomic ratio C/Si = 0.85, are investigated in a wide frequency and temperature range. Two samples, namely S1400 and S1700, obtained from the same synthesis batch but submitted to annealing at, respectively, 1400 and 1700 °C, are representative of this class of material. In particular, quasi-insulating and semiconducting states are evidenced in these samples, and they point out the influence of the annealing treatment. The dielectric spectra of S1400 are marked by a relaxation process and by a thermally activated conductivity, whereas only a large dc-conductivity is found in the S1700 sample. The temperature dependence of both relaxation times and dc-conductivity are determined and interpreted taking into account the transport process in these media. EPR investigations are carried out to correlate the electrical and dielectric behaviour with the surface states of the nanoparticles which exhibit heterogeneous composition and surface active electronic centres. The experimental conductivity and dielectric functions in these silicon-rich materials are discussed and compared with those from carbon-rich np-SiC samples.

(Some figures in this article are in colour only in the electronic version)

1. Introduction

Mostly known for their good mechanical and thermal properties [1–3], silicon carbide (SiC) materials in their nanosized structure also have interesting dielectric and electrical properties [4, 5] which are different from those of the bulk material. The synthesis of SiC

[3] Author to whom any correspondence should be addressed.

nanopowders is achieved by a laser pyrolysis of SiH_4 and C_2H_2 gaseous mixture as described elsewhere [6, 7]. Depending on the initial ratio of the gaseous mixture, the final network contains either an excess of carbon or silicon. The excess is arranged as isolated clusters in a weak proportion or associated with the SiC at the grain surfaces [8]. The interesting feature is the modulation of the physical properties to a large extent by a suitable annealing treatment [2, 3, 9]. In fact, the nanoparticles can be obtained with a narrow grain size distribution ranging from 10 to 100 nm by annealing treatment [10]. Thus, variable dielectric permittivity and electrical conductivity can then be obtained depending on the application needs. Our previous work carried out on the batch of SiC nanoparticles (referred to as SiC212) containing an excess of carbon [5] have shown that the static dielectric permittivity varies by one order of magnitude by changing the annealing temperature from 1400 to 1700 °C. In the meantime, the dc-conductivity increases by several orders of magnitude up to 0.05 S cm^{-1} [5, 10]. This study has demonstrated the ability of dielectric spectroscopy to investigate interfacial polarization phenomena involved at the SiC nanoparticle (np-SiC) boundaries. On the other hand, EPR spectroscopy is a suitable technique for probing the unpaired spins which can be associated with the involved charge carriers in the nanoparticles core or at their outermost surfaces. Therefore, in order to clarify the influence of the stoichiometry and interface effects on the overall polarization and conduction mechanism, we have carried out dielectric and EPR studies on nanopowders characterized by an excess of silicon. If the np-SiC core retains its stoichiometry and crystalline structure as involved in the bulk SiC, the outermost particle surface exhibits a silicon-rich composition [11, 12]. The chemical bonding (surface reconstruction, heterogeneous composition, dangling bonds) at the interfaces play a key role on the interfacial polarizations between the nanoparticles and hence the electrical and dielectric behaviour of the nanopowders. In these nanosized materials, the relevant data such as the relaxation times and the conductivity are determined and discussed with regard to the surface states and the annealing effect.

2. Experimental details

2.1. Materials

Nanosized SiC powders were synthesized by laser pyrolysis of SiH_4 and C_2H_2 mixture following the experimental procedure reported elsewhere [6, 7]. Two SiC powders were investigated: namely S1400 and S1700, annealed respectively at 1400 and 1700 °C, for 1 h under argon. They are representative of the batch of SiC nanoparticles (referred to as SiC218) which is characterized by an excess of silicon in the atomic ratio $C/Si = 0.85$ obtained from the initial composition of the gaseous reactants. Such excess is arranged as isolated silicon clusters or associated to the particle surfaces. As a matter of fact, the SiC nanoparticles are coated by a thin layer (0.5–1.0 nm thick) of oxide and exhibit silicon-rich composition at the outermost particle surface. Details of the morphological and structural features of the SiC218 annealed at 1400 °C (S1400) are illustrated by the high resolution transmission electron microscopy image depicted in figure 1(a) and by solid state NMR of ^{29}Si (figure 1(b)). The nanocrystal boundaries exhibit diffused shapes because of the amorphous structures and heterogeneous composition of the external SiC layers. In contrast, well defined crystalline order is clearly seen in the np-SiC cores. The nanoparticle sizes exhibit a relatively narrow distribution in the range $\langle d \rangle = 25$ nm $\pm$ 5 nm. From the NMR spectrum of S1400, we may notice the coexistence of the crystalline polytypes 3C-SiC (cubic), 6H-SiC (hexagonal) and a fraction of amorphous structure which can result either from the disorder at the particle boundaries or to stacking faults in the nanoparticle cores. The annealing treatment leads to a coalescence of

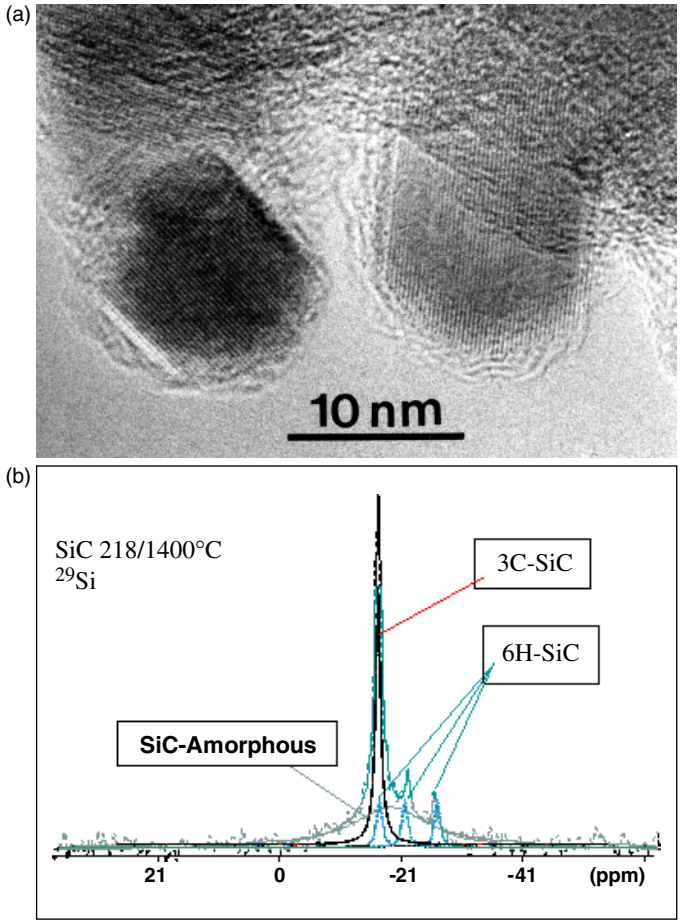

Figure 1. (a) High resolution transmission electron microscopy image of the S1400 sample. The nanoparticle surface is marked by silicon in excess while a good crystalline order is realized in the nanoparticle core. (b) ^{29}Si solid state NMR spectrum of the SiC218 sample annealed at 1400 °C. The different polytypes 3C-SiC (single NMR line), 6H-SiC (triplet NMR lines) and amorphous fraction (broad NMR line) of the sample are also indicated.

the nanoparticle and to an improvement of the crystalline order. Similar structural behaviours were already observed in carbon-rich samples [10].

2.2. Dielectric relaxation spectroscopy

Dielectric measurements were performed over a wide frequency range (0.1 Hz–3 MHz) at different temperatures between 153 and 473 K using a Novocontrol Broadband Dielectric Spectrometer [13]. In the given frequency range, a Solartron SI1260 combined with a Broadband Dielectric Converter (BDC) allows impedance and dielectric measurements. The dielectric device was coupled to a Quatro temperature controller. Isothermal measurements were carried out on a sufficient amount of powder samples adjusted between the electrodes of a Novocontrol BDS 1309 dielectric sample cell specially designed for liquids and powders (figure 2). The excess of powder which does not fit between the electrodes can flow around the upper electrode. With this sample cell configuration, the sample thickness is determined

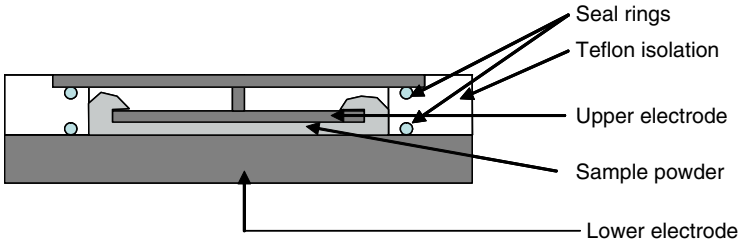

Figure 2. The powder sample cell configuration with the geometrical dimensions reported in the text.

by the upper electrode used. The thickness was 1 mm and the diameter of the upper electrode was 20 mm. The temperature was measured in the immediate neighbourhood of the sample with accuracy better than ±0.1 K.

2.3. EPR spectroscopy

A Bruker spectrometer was used for the conventional CW-EPR investigations in the X band (9.5 GHz). Variable temperature studies were performed by using an Oxford Instrument cryostat which allows temperature stabilization within ±0.02 K from room temperature down to 4 K. The EPR investigations were performed by using typical amounts (about 20 mg) of powder introduced in an EPR quartz tube. Due to the high concentration of paramagnetic species, low microwave powers (<2 mW) and low modulation fields (<0.5 G) were typically used to record the EPR spectra far from saturation conditions. The relative paramagnetic centre concentrations were determined from the unpaired spin susceptibility obtained by a double integration of the EPR spectra.

3. Experimental results

3.1. Dielectric functions

The real and imaginary parts of the dielectric function were recorded versus the frequency and the temperature. The samples S1400 and S1700 were found to be representative of the silicon-rich batch with regard to their quasi-insulating and semiconducting states, respectively. These features are taken into account through the frequency dependence of the complex dielectric permittivity according to the Havriliak–Negami (HN) phenomenological equation [14, 15]:

$$\varepsilon^* = \frac{\sigma_{dc}}{i\omega\varepsilon_0} + \varepsilon_u + \frac{\Delta\varepsilon}{(1 + (i\omega\tau)^\alpha)^\beta}. \tag{1}$$

This approach was used to model the experimental results and allows the determination of the relaxation time τ, the associated distribution parameters α and β representing, respectively, the symmetrical and asymmetrical broadening of the dielectric functions. The first term in equation (1) depends on the steady state conductivity σ_{dc} while ε_0 is the vacuum permittivity and the dielectric strength $\Delta\varepsilon$ represents the difference between the low (relaxed) frequency dielectric permittivity and the high (unrelaxed) frequency one (ε_0).

The frequency and thermal behaviour of the real and imaginary parts of the dielectric permittivity in S1400 sample are depicted respectively in figures 3(a), (b). Two dispersion regimes are clearly revealed in the curve shapes. They consist of the low frequency dispersion (LFD) and the high frequency one (HFD). From the real permittivity graph, we may note the high amplitude of the LFD due to polarization phenomena involved at the electrodes or at

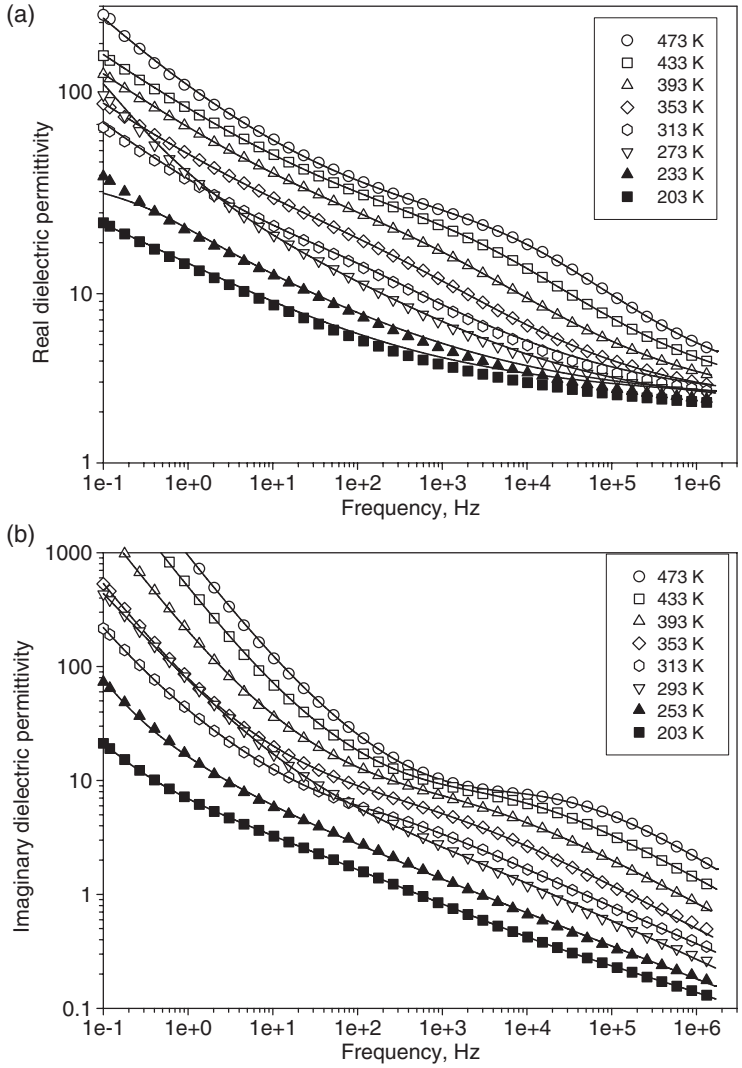

Figure 3. Frequency dependence of the real (a) and imaginary (b) parts of the dielectric permittivity at different temperatures in SiC nanopowders annealed at 1400 °C (S1400 sample). The solid lines are the best fit to the HN equation.

the nanoparticle interfaces, while the LFD on the imaginary part results from the steady state conductivity as supported by the first term of the HN equation. On the other hand, the HFD represents a relaxation process associated with the charge carriers' mobility.

At high temperatures (above 213 K), the LFD and HFD curves are well separated and adjusted by the HN equation with a good accuracy. A symmetrical distribution of the HFD relaxation times was found by fitting the data to equation (1) with the values $\alpha = 0.5$ and $\beta = 1$. Whatever the sample temperature, these parameters remain constant, in contrast to the dielectric strength, which increases with the sample temperature.

However, at temperatures below 213 K, the LFD signature is partially overlapped with the high frequency relaxation process. The overlapping degree increases with decreasing the

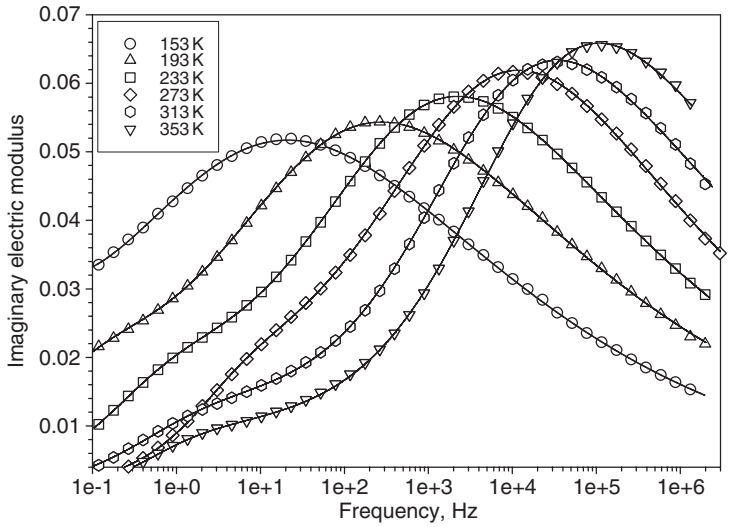

Figure 4. Frequency dependence of the imaginary part of the electrical modulus at different temperatures in SiC nanopowders annealed at 1400 °C (S1400 sample). The solid curves are the best fit to the imaginary part of the HN equation.

temperature, leading to inaccurate adjustment of the experimental curves by HN equation. So, in order to account correctly for the temperature dependence of the relaxation time in the entire temperature and frequency ranges, the electrical modulus formalism and the corresponding representation were preferred for the determination of the HFD relaxation times. As far as the present report is concerned, the advantage of this representation is to minimize the LFD shape and to enhance the high frequency one. This approach is highly relevant for the separation of the two processes and for an improvement of the HN model adjustment to the relaxation curves in these materials. The imaginary component M'' is defined by the dielectric function parameters according to the formula

$$M''(\omega) = \frac{\varepsilon''(\omega)}{\varepsilon'^2(\omega) + \varepsilon''^2(\omega)}. \tag{2}$$

The results of M'', depicted in figure 4, show clearly two peaks related to the LFD and HFD processes. The LFD on the imaginary dielectric permittivity evolution is transformed to a peak with low amplitude according to the well established behaviour in the modulus formalism [16]. The opposite situation is observed for the HFD being associated with a high amplitude peak. The temperature dependence of the modulus relaxation times reported in figure 4 was determined by fitting M'' spectra to equation (1) assuming two relaxation processes.

To sum up, we may note the relevant information from the dielectric function marked by the LFD and HFD relaxation processes in np-SiC with silicon in excess. This is valid only for the S1400 sample while the large dc-conductivity in S1700 overcomes any observation of relaxation processes in the considered frequency range. The HN model accounts accurately for the main features of the experimental results in the S1400 sample. However, the modulus formalism leads to appropriate representations of the dielectric function results and allows better simulations by the HN equation in the entire temperature and frequency ranges.

3.2. Surface electronic active centres probed by EPR

EPR measurements in nanosized materials are relevant for pointing out the origin of the charge carriers and the surface states from the unpaired spins. Indeed, high specific surfaces of nanoparticles favour the creation of surface unsaturated electronic bonds. Following the nature of the external surface composition and for an energy criterion, the chemical bonding can be adjusted to limit the concentration of dangling bonds. This fact was clearly shown in the case of carbon-rich materials [8, 10, 11] where the surface dangling bonds are no longer involved. In the present case with np-SiC surfaces marked by silicon in excess, the main features of the EPR spectra are shown in figure 6 for the S1400 sample. These results are consistent with surface active paramagnetic centres which interact drastically with ambient atmosphere or with a partial oxygen pressure. Indeed, the paramagnetic oxygen interacts with the dangling bonds at the nanoparticle surfaces, leading to the relaxation of the paramagnetic centres. These interactions are traduced on the EPR spectra shapes through line broadening in the S1400 sample. However, no such oxygen effect was found in the S1700 sample. This observation can be explained by the fact that electronic active centres are no longer involved at the nanoparticle surfaces for high annealing temperature (1700 °C). Moreover, the annealing effect can be monitored from the unpaired spin susceptibility which is deduced from the double integration of the EPR spectra. The results, summarized in figure 7, show the drastic reduction of the unpaired spin concentration when the annealing temperature increases. Analysis of the thermal evolution of the spin susceptibility (χ) (figure 7(b)) in the S1700 sample shows that the involved paramagnetic centres are not localized (failure of the Curie–Weiss law $\chi * T =$ constant). A delocalization inside the nanoparticle core with short relaxation times is plausibly the origin of the decrease in the ($\chi * T$) with the rise of the sample temperature. The involved paramagnetic centres constitute the physical support of the conduction phenomena in the S1700 sample.

4. Discussion

The thermal evolution of the dielectric function is marked by the critical temperature $T_c = 313$ K. An attempt to interpret the dielectric relaxation and conductivity results within the framework of thermal activation laws such as that relevant in a variable range hopping process [17] or that used in SiC fibbers [18] fails. Hence, the temperature dependence of the HFD relaxation time of M'' (figure 5) and the dc-conductivity are accounted for, above and below the critical temperature $T_c = 313$ K, by means of Arrhénius law as follows:

$$\tau = \tau_0 e^{E/kT} \tag{3}$$

and

$$\sigma_{dc} = \sigma_0 e^{-E/kT} \tag{4}$$

where k represents the Boltzmann constant, E is the activation energy, T the sample temperature and τ_0 and σ_0 represent the relaxation time and conductivity, respectively, at very high temperature.

In the S1400 sample, the following values ensure the best fit of the relaxation time:

For $T < T_c$: $\tau_0 = 2 \times 10^{-9}$ s $E/k = 2423$ K

For $T > T_c$: $\tau_0 = 1.87 \times 10^{-11}$ s and $E/K = 3918$ K.

The electrical conductivity involved in S1400 and S1700 is deduced from the imaginary dielectric permittivity as follows:

$$\sigma' = \omega \varepsilon_0 \varepsilon''. \tag{5}$$

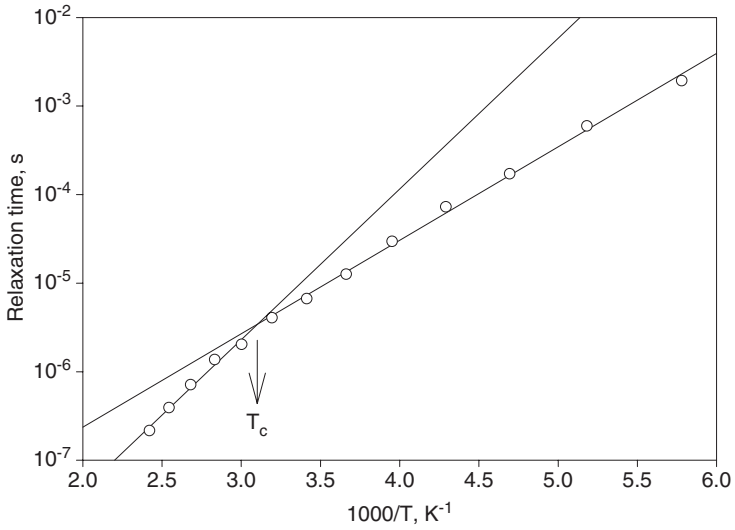

Figure 5. Temperature dependence of the relaxation time in the SiC nanopowders annealed at 1400 °C (S1400 sample). The solid lines are fits to an Arrhénius law.

The frequency dependence is depicted in figures 8(a) and (b) respectively for the S1400 and S1700 samples. The S1400 dc-conductivity, which appears in the experimental frequency window only at temperatures higher than T_c, is accounted for by the activation law (equation (3)) with a pre-factor $\sigma_0 = 2.9 \times 10^{-6}$ S cm^{-1} and an activation energy $E/k = 4089$ K; i.e. of the order of that determined from the relaxation time. This result suggests an inverse proportionality between the relaxation time and the dc-conductivity in the temperature range above T_c according to the following relation:

$$\sigma_{dc}\,(T > T_C) = \frac{\varepsilon_0 \varepsilon_s}{\tau\,(T > T_C)} \tag{6}$$

with ε_0 and ε_s corresponding, respectively, to the vacuum permittivity and the low frequency permittivity of the sample. The obtained dependence is consistent with the transport mechanism in these nanopowders being characterized by the couple (σ_{dc}, τ). It is worth noting that this proportionality is encountered in electronic [19, 20] and ionic conductors as well [16, 21, 22].

In the S1700 sample, as shown in figure 8(b), only dc-conductivity is observed without any relaxation process in the considered frequency range. This is in agreement with the relation (equation (6)) since the relaxation peak should be shifted to higher frequency regarding the higher dc-conductivity compared to that in S1400 sample. Thus, the most drastic change occurs in the electrical behaviour by increasing the annealing temperature from 1400 to 1700 °C. Furthermore, the thermal variation of the S1700 dc-conductivity (figure 9) is similar to the HFD relaxation time in S1400 where two distinct regimes are also observed with the same cross-over temperature T_c. The activation energies of both regimes $E/k = 220$ K for $T < T_c$ and $E/k = 522$ K for $T > T_c$ are dramatically reduced compared to those of S1400. Meanwhile, a drastic increase of the conductivity is induced by higher annealing temperature and the thermal variation of the dc-conductivity in S1700 is as follows:

$$T > T_c: \qquad \sigma_0 = 0.66 \times 10^{-3}\ \text{S cm}^{-1}, \qquad E/k = 522\ \text{K}$$
$$T < T_c: \qquad \sigma_0 = 0.26 \times 10^{-3}\ \text{S cm}^{-1}, \qquad E/k = 220\ \text{K}.$$

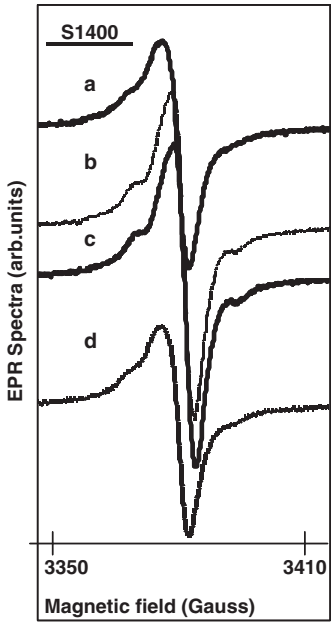

Figure 6. Effect of oxygen on the EPR spectra in the silicon-rich SiC sample annealed at 1400 °C (S1400). The EPR spectra were recorded in the following conditions: (a) under air, (b) under 1 atm partial pressure of oxygen, (c) under low partial pressure of oxygen (200 mTorr), (d) under vacuum. The changes on the EPR spectra intensity and line shape reflect the interaction between (paramagnetic) oxygen and the active dangling bonds at the SiC nanoparticle surfaces.

The energy value around $E/k = 220$ K is of the order of that inferred from EPR studies. Indeed, the thermal variation of the unpaired spin susceptibility in the S1700 sample (figure 7(b)) exhibits an activation energy of about $E/k = 120$ K. This value is interpreted as the binding energy of individual charges to their local sites in the nanocrystallite core. Furthermore, the existence of the two activation energy levels in the conductivity graph suggests that two conduction channels are involved in these materials. The one associated with the low energy may correspond to charge carrier motions inside the nanoparticles, in agreement with EPR measurements. Above T_c, an additional contribution to the conductivity may arise from inter-grain conductivity when the thermal energy of the charge carriers is high enough to overcome the energy barriers at the interfaces.

The difference in the activation energy values between S1400 and S1700 can be explained by the structural changes induced by annealing treatment of the nanoparticles. In particular, annealing at 1700 °C increases the grain sizes with an improvement of the crystalline order and a lowering of the thickness of the outermost silicon-rich surfaces. All these effects contribute to lower the energy of the inter-grain barriers.

Finally, let us draw below the main concluding remarks on the dielectric and conduction features in silicon-rich nanoparticles compared to those of carbon-rich nanopowders [5].

- At the early stage of the annealing treatment, i.e. at 1400 °C, the stoichiometry effects are important both on the chemical composition of the outermost particle surfaces and on the surface electronic active centres (dangling bonds). In the carbon-rich sample, the surface is relatively inert due to the carbon sheets which adjust on the nanoparticle surfaces [8]. The turbostratic carbon bonding [8] prevents the formation of surface dangling bonds.

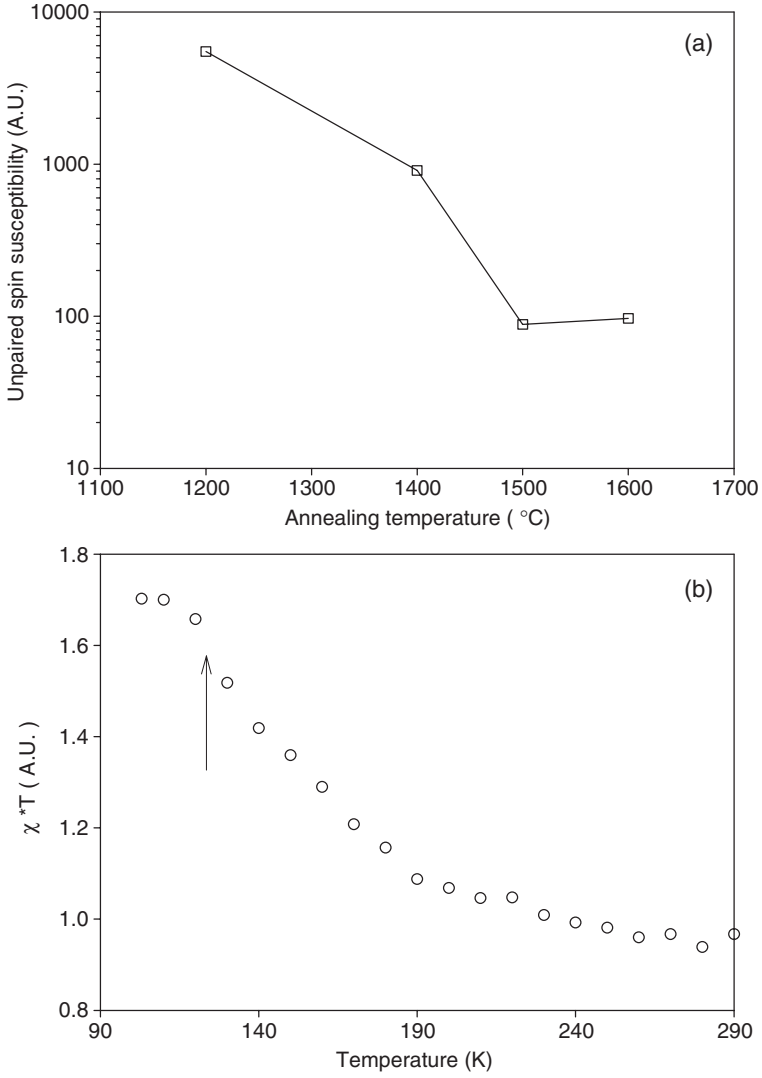

Figure 7. Paramagnetic spin susceptibility versus the annealing temperature (a) and the thermal evolution of the S1700 sample susceptibility (b). The arrow indicates a characteristic temperature for the delocalization of the unpaired spins associated with charge carriers in the nanoparticles.

In that sample, the static relative dielectric permittivity ($\sim$100) is twice as large as the value in silicon-rich samples. This result is of primary importance and points out the interfacial polarization involved at the grain surfaces. In contrast, the silicon-rich sample exhibits surface electronic active centres which compete with the polarization effects through charge combination, suppressing then the surface dangling bonds and limiting the polarization strength.

- Concerning the effective dc-conductivity, the activation energy is larger in the carbon-rich systems due to the strength of the interfacial polarization. Meanwhile, the pre-factor of the dc-conductivity is about several orders of magnitude lower in the silicon-rich sample. As a matter of fact, electronic active centres at the interfaces limit the interfacial polarization

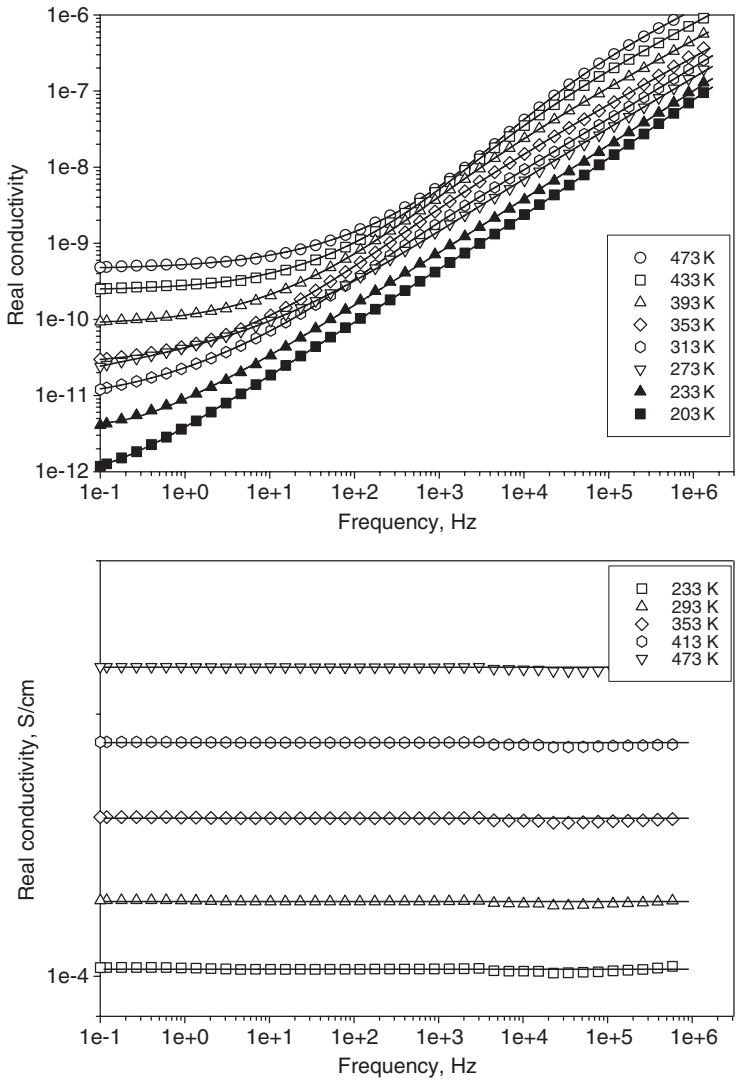

Figure 8. Frequency dependence of the real electrical conductivity at different temperatures in SiC nanopowders annealed at 1400 °C (a) and in the S1700 sample (b).

and act as charge traps which prevent the inter-grain flow of charge carriers, limiting the effective conductivity in the silicon-rich sample.

- For the higher annealing temperature (1700 °C), a better homogeneity of the structural order and the surface states is obtained. Whatever the species in excess (carbon, silicon) at the surfaces, the removal of this excess by annealing at 1700 °C and then limiting its role on the physical properties of the nanopowders. Thus, the electrical and dielectric behaviours exhibit common features whatever the initial composition of the sample. As a consequence, both the activation energy of the charge carriers and the magnitude of the effective dc-conductivity are similar in both systems.

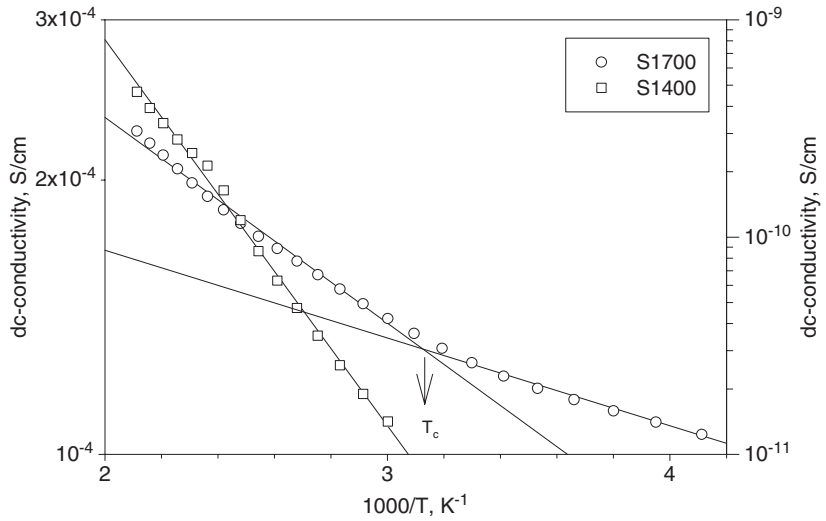

Figure 9. Temperature dependence of the dc-conductivity in the SiC nanopowders annealed at 1400 °C (S1400 sample) and 1700 °C (S1700 sample). The solid lines are the best fit to an Arrhénius law.

5. Conclusions

The main results reported in this study concern the drastic changes in the electrical and dielectric properties induced by annealing in non-stoichiometric SiC nanosized powders. The nanoparticles with an excess of silicon exhibit reactive surfaces due to dangling bonds as probed by EPR under oxygen pressure. More inert surfaces seem to be realized in the nanopowders with an excess of carbon located at the outermost particle surfaces. In the present study on silicon-rich nanoparticles, the dc-conductivity increases by six orders of magnitude on increasing the annealing temperature from 1400 to 1700 °C. In both samples S1400 and S1700, electrical conductivity proceeds, at least, from two conduction mechanisms corresponding to quite different activation energies. Polarization at the interfaces and charge carriers in the nanoparticle cores coexist in the nanomaterials. The charge carriers in the nanoparticle cores were already demonstrated by Hall measurements in carbon-rich samples [10]. In the silicon-rich powders, the electronic active centres probed by EPR are involved at the nanoparticles surfaces and they play a key role in the reduction of the interfacial polarization strength and on the charge carriers' channels in silicon-rich media. These effects are of particular importance in the early stage of annealing (1400 °C), while a higher temperature (1700 °C) give rise to a better homogeneity of the samples, leading to similar electrical properties whatever the initial composition of the SiC nanomaterials.

Acknowledgments

The authors are grateful to Dr M Mayne (CEA—Saclay—France) for the synthesis of silicon-rich SiC nanoparticles and to Dr S Kodjikian (LDOF—Le Mans-France) for the transmission electron microscopy images. Pr J Emery (LPEC—Le Mans) is acknowledged for the NMR spectra of silicon carbide nanomaterials.

This work has benefited from the bilateral agreement facilities between the Université du Maine (Le Mans—France) and Jan Dlugosz University (Czestochowa—Poland).

References

[1] Niihara K and Nakahira A 1991 *Ann. Chim. Fr.* **16** 479
[2] Monthioux M and Delverdier O 1996 *J. Eur. Ceram. Soc.* **16** 721
[3] Karlin S and Colomban Ph 1998 *Composites* B **29** 41
[4] Kassiba A and Charpentier S 2002 *Nanostructured Silicon Based Powders and Composites* (London: Taylor and Francis) chapter 5
Kassiba A 2002 *Nanostructured Silicon Based Powders and Composites* (London: Taylor and Francis) chapter 6
[5] Kassiba A, Tabellout M, Charpentier S, Herlin-Boime N and Emery J R 2000 *Solid. State Commun.* **115** 389
[6] Yajima S 1980 *Phil. Trans. R. Soc.* A **294** 419
[7] Cauchetier M, Croix O and Luce M 1988 *Adv. Ceram. Mater.* **3** 147
[8] Charpentier S, Kassiba A, Bulou A, Monthioux M and Cauchetier M 1999 *Eur. Phys. J.* **8** 111
[9] Mouchon E and Colomban Ph 1996 *J. Mater. Sci.* **31** 323
[10] Charpentier S, Kassiba A, Emery J and Cauchetier M 1999 *J. Phys.: Condens. Matter* **11** 4887
[11] Kassiba A, Makowska-Janusik M, Bouclé J, Bardeau J-F, Bulou A, Herlin-Boime N, Mayne M and Armand X 2002 *Diamond Relat. Mater.* **11** 1243
[12] Kassiba A, Makowska-Janusik M, Bouclé J, Bardeau J-F, Bulou A and Herlin-Boime N 2002 *Phys. Rev.* B **66** 155311–7
[13] Kremer F and Arndt M 1997 *Dielectric Spectroscopy of Polymeric Materials* ed J P Runt and J J Fitzgerald, American Ceramic Society, chapter 2
[14] Havriliak S Jr and Havriliak S J 1997 *Dielectric and Mechanical Relaxation in Polymers* (Washington, DC: Hanser) chapter 1
[15] Havriliak S and Negami S 1996 *J. Polym. Symp.* **14** 89
[16] Macedo P B, Moynihan C T and Bose R 1972 *Phys. Chem. Glasses* **13** 171
[17] Mott N F and Davis E A 1979 *Electronic Process in Non-crystalline Materials* (Oxford: Clarendon)
[18] Chauvet O, Stoto T and Zuppiroli L 1992 *Phys. Rev.* B **46** 8139
[19] Pelster R, Nimtz G and Wessling B 1994 *Phys. Rev.* B **49** 12718
[20] Hunt A 1993 *J. Non-Cryst. Solids* **160** 183
[21] Moynihan C T 1994 *J. Non-Cryst. Solids* **172–174** 1395
[22] Arulraj A, Goutenoire F, Tabellout M, Bohnke O and Lacorre P 2002 *Chem. Mater.* **14** 2492